Noname manuscript No.
(will be inserted by the editor)

A physically based model of the effect of recovery and clustering on recrystallization kinetics

Partha Sarathi De · Amol Vuppuluri · V. Subramanya Sarma · Srikanth Vedantam

Received: date / Accepted: date

Abstract The classical JMAK model of recrystallization kinetics has been widely used to describe the growth of randomly distributed nuclei under constant driving force. These conditions are not satisfied in many systems. The driving force for growth generally varies with time, and the nuclei are usually not uniformly distributed. In this paper, we present a physically motivated alternative model of recrystallization kinetics, which accounts for the variation of driving force due to recovery and the effect of clustering of the nuclei. The model is based on the growth kinetics of initially circular, strain free nuclei in a deformed matrix. The effect of recovery on the recrystallization kinetics is studied in terms of the parameters governing initial stored energy and the decay rate. The model predicts cessation of recrystallization when the stored energy decreases below a certain critical limit. This cessation depends on both the initial stored energy value as well as the recovery time constant. The effect of clustering of nuclei on recrystallization kinetics is analyzed by considering representative volume elements with different nuclei distributions. It is shown that recrystallization kinetics becomes slower with increased clustering. The results of this mean field model are compared to phase field simulations.

Partha Sarathi De · Srikanth Vedantam
Department of Engineering Design
Indian Institute of Technology Madras
Chennai 600036, India
E-mail: prodpartha13@gmail.com of Partha Sarathi De
E-mail: srikanth@iitm.ac.in of Srikanth Vedantam

Amol Vuppuluri
Department of Mechanical Engineering
Birla Institute of Technology and Science-Pilani, Hyderabad Campus
Telangana, 500078, India E-mail: amol@hyderabad.bits-pilani.ac.in

V. Subramanya Sarma
Department of Metallurgical and Materials Engineering
Indian Institute of Technology Madras
Chennai 600036, India E-mail: vsarma@iitm.ac.in

Keywords Recrystallization kinetics · Mean field model · Recovery rate · Nuclei clustering

1 Introduction

In metals and alloys, the formation of polycrystalline microstructure during high temperature annealing post deformation is termed as static recrystallization. This process is of great technological importance and has been studied extensively for many decades [1, 2, 3, 4]. At elevated temperatures, relatively strain free regions in deformed material become nuclei, which grow and consume the surrounding strained material. The stored energy difference between the deformed regions and the strain free nuclei drives the growth of the nuclei.

The kinetics of the recrystallization process in metals has generally been described by the classical Johnson-Mehl-Avrami-Kolmogorov (JMAK) theory [1]. While this theory has been applied to a wide variety of systems [5, 6, 7], it is based on the assumptions of *randomly distributed constant growth rate of the nuclei* and can include both site saturated nuclei and constant nucleation rate. Under these idealized assumptions, this model predicts that the recrystallization fraction X is given as a function of time t in the form $X(t) = 1 - \exp(-Kt^n)$ where K is a constant and n is generally referred to as the Avrami exponent. Most materials do not appear to conform to JMAK kinetics [8, 9, 10, 5]. The reasons have been variously attributed to non-constant driving force [11, 8], non-uniformly distributed nuclei [3, 12, 13], inhomogeneity of the stored energy [14, 15] and pinning by second phase particles [11].

During recrystallization, the stored energy in the highly deformed regions decreases with time due to a concurrent process, termed recovery. This process reduces the driving force for recrystallization [4, 11]. The strain free nuclei are also generally not uniformly distributed in many systems [12, 13]. For a given area density of nuclei, the nuclei could be clustered in some locations, and the clusters could be spread out. As a result, the growing nuclei impinge upon their neighbours in the cluster before impingement on neighbouring clusters. This process affects the kinetics of the recrytallization process [3]. Storm and Jensen [12] have performed a recrystallization simulation of a clustered distribution of nucleation sites, which was observed experimentally in 90% cold-rolled aluminum (AA1050) material. Their simulations revealed that clustering changes the recrystallization kinetics, recrystallized microstructural morphology and the grain size distribution. Villa and Rios [13] considered Matern cluster processes to characterize such clustered nucleation and obtained analytical solutions of the recrystallization kinetics by employing stochastic approaches. Their rigorous mathematical analysis indicates that the effect of different Matern cluster process parameters, cluster radius R, the intensity of the parent Poisson process λ_p and mean number of points per cluster n_c strongly affect the recrystallization kinetics.

Several models have been developed to consider the effect of non-constant driving force on the recrystallization kinetics [8, 16, 17, 18]. Of these, the

models developed by Speich and Fisher [16] and Vandermeer and Rath [8] are notable. While the JMAK model uses an extended volume approach to account for the effect of impingement between adjacent recrystallized grains for recrystallized fraction calculation, these models are based on an empirical calculation of the impinged interface area. All these models use an assumption of random distribution of nuclei and have been extended in many other studies [19, 20, 21, 22]. In this work, we develop a simple two dimensional, physically motivated model to study the effect of both non-constant driving force and clustering on recrystallization kinetics based on a mean-field approach. We note that a non-constant driving force has been incorporated into the JMAK approach through a *post facto* modification of the JMAK kinetics derived from the assumption of a constant driving force [11]. In contrast, we present a simple model capable of describing isothermal recrystallization kinetics based on the time dependent driving force. We base our model on a mean-field description of recrystallization, which was proposed by our group [23]. The model was based upon the assumption of a uniform distribution of strain free nuclei in a highly deformed matrix. The nuclei were assumed to grow with first order kinetics driven by both curvature and stored energy difference. The stored energy was taken to vary with time in the form $E_{st} = E_0 + E_1 \exp\left(-\frac{t}{\tau}\right)$ where τ is the time constant of recovery. However, the previous work only considered the kinetics up to the impingement of the nuclei and considered an initially uniform distribution of the nuclei. In this paper, we first extend the mean field model to study the complete post impingement recrystallization kinetics. We also develop a model of clustered nucleation using a representative volume element (RVE) approach. We then systematically study the effect of the initial stored energy and the recovery time constant on recrystallization kinetics — particularly on the Avrami exponent. We find that recrystallization ceases for certain combinations of the initial stored energy and the recovery time constant. We introduce a clustering parameter, which is a ratio of the distance between adjacent nuclei and the size of the RVE. The effect of the clustering parameter on the Avrami exponent is studied. Finally, we compare our model with a phase field model to contextualize our results. A multiorder parameter phase field model based on the work of Fan and Chen [24] has been used. The coarse grained free energy of the classical phase field model is modified to account for the stored energy driven recrystallization [23]. This paper is organized as follows: Section 2 presents a description of the model for both the uniform and non-uniform distribution of the nuclei. The assumptions are described, and the analytical approach is presented. Section 3 describes the results obtained from the proposed model and a discussion of their significance. Finally, the conclusions are summarized in Section 4.

2 Model Description

As mentioned in the introduction, the mean field model is based on the first order kinetics of nuclei growth driven by curvature and stored energy differ-

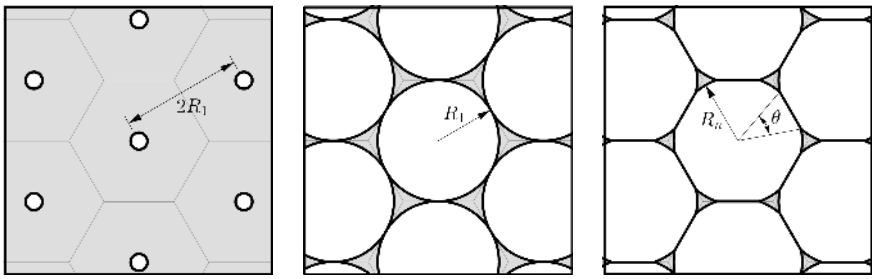

Fig. 1 Different stages of growth during recrystallization: (a) Distribution of the initial nuclei in two dimensions, (b) impingement of the growing grains and (c) growth after impingement.

ences. Following [23], we summarize the model below. The rate of growth of a nucleus is given by

$$\frac{dR}{dt} = M\left(-\frac{\gamma}{R} + E_{st}(t)\right), \tag{1}$$

where the stored energy difference is taken to be of the form $E_{st} = E_0 + E_1 \exp\left(-\frac{t}{\tau}\right)$. For ease of parametric analysis we consider the dimensionless form of Eq. (1) in the form

$$\frac{d\bar{R}}{d\bar{t}} = -\frac{1}{\bar{R}} + 1 - \xi + \xi \exp^{-\bar{t}/\bar{\tau}}, \tag{2}$$

where $\bar{R} = R(t)/R_c$, $\bar{t} = ME_i t/R_c$, $\xi = E_1/E_i$, $\bar{\tau} = ME_i\tau/R_c$ with initial stored energy $E_i = E_0 + E_1$. The critical nucleus size is $R_c = \gamma/E_i$ which can be obtained by setting dR/dt to zero at $t = 0$ in Eq. (1). Thus, a competition between the grain boundary energy γ and initial stored energy E_i determines the critical nucleus size as in the classical nucleation theory. Equation (2) is solved numerically to obtain the radius of the nucleus as a function of time, assuming a uniform distribution of nuclei. Figure 1 shows the distribution of nuclei in a deformed matrix (grey region) and their subsequent growth as strain free grains (white regions). The nuclei are taken to be in a hexagonal arrangement in the deformed matrix. The growth of the grains leads to impingement (Fig. 1b) between growing grains. A detailed calculation of recrystallized fraction based on these assumptions is given in Appendix A.

2.1 Clustering of nuclei

Next, we describe the model for clustered nuclei. For this, we consider clustering in hexagonal RVEs. The distribution of nuclei for analyzing the clustering effect is shown in Fig. 2. The overall distribution of nuclei is obtained by periodically placing a cluster of three nuclei in each hexagon of a hexagonal grid (Fig. 2a). The ratio of two characteristic lengths: r_3 and R_3, identified

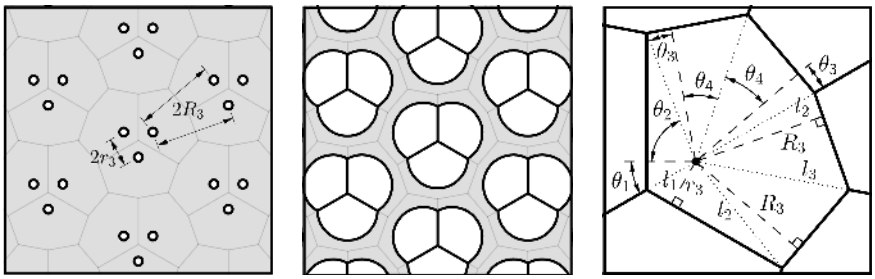

(a) (b) (c)

Fig. 2 Representative volume elements of the recrystallization process with clustered nuclei: (a) initial distribution of the nuclei, (b) impingement of local clusters and (c) final grain shapes. The dimensions are defined by $\theta_1 = \frac{\pi}{6}, \theta_2 = \arccos\frac{r_3}{2R_3} - \sin^{-1}\frac{r_3}{2R_3}, \theta_3 = \sin^{-1}\frac{r_3}{2R_3}, \theta_4 = \frac{\pi}{6}, l_1 = \frac{2r_3}{\sqrt{3}}, l_2 = \frac{2{R_3}^2}{\sqrt{4{R_3}^2 - {r_3}^2}}, l_3 = \frac{2R_3}{\sqrt{3}}$.

in Fig. 2a, is used to define a clustering ratio C_r. When $C_r = 1$, the nuclei are uniformly distributed with no clustering. In the clustered distribution, each growing grain impinges on six surrounding grains at two different radii of curvatures, r_3 and R_3, respectively.

In the first occurrence of impingement (with a radius of curvature r_3), concurrent impingement with two other grains from the same cluster takes place. After this impingement, the entire cluster is assumed to grow. In the second impingement between adjacent clusters, the four grains from nearby clusters impinge, and this takes place simultaneously with the radius of curvature of the grain being R_3. Figure 2b shows the grain boundary shape after the first local impingement. After complete recrystallization, each nucleus is assumed to take a final shape that is presented in Fig. 2c. The clustering ratio determines this final shape. This final shape can be considered as a representative element for the calculation of recrystallized volume fraction. If the current radius of curvature, denoted by R_n, lies between l_2 and l_3 (Fig. 2), then the recrystallized area in a single representative element can be expressed as

$$\begin{aligned} A_{rec} = & \int_0^{r_3} 2\pi R dR + \int_{r_3}^{l_1} \left(2\pi - 4\arccos\frac{r_3}{R}\right) R dR \\ & + \int_{l_1}^{R_3} \left(2\pi - 2\theta_1 - 2\arccos\frac{r_3}{R}\right) R dR \\ & + \int_{R_3}^{l_2} \left(2\pi - 2\theta_1 - 2\arccos\frac{r_3}{R} - 8\arccos\frac{R_3}{R}\right) R dR \\ & + \int_{l_2}^{R_n} \left(2\pi - 2\theta_1 - 2\theta_2 - 4\theta_3 - 4\arccos\frac{R_3}{R}\right) R dR. \end{aligned} \tag{3}$$

All the parameters in the above equation are defined in Fig. 2c. The limits in the integration terms of Eq. (3) represents the radius of curvature at various

transition points of the impingement. There are successive steps in the domain of R, and the terms of the integration are different in each step. To obtain the value of A_{rec}, the integration is performed using the value of the current radius of curvature R_n. The area of the representative element, which is the maximum value of A_{rec}, is calculated by integrating up to the maximum value of $R_n = l_3$.

The area of the representative element is given as $A_c = \frac{2R_3}{\sqrt{3}} + \frac{r_3}{\sqrt{3}} + r_3\sqrt{4{R_3}^2 - {r_3}^2}$ in the case of nonuniform clustering. Subsequently, the recrystallized area fraction X_r is calculated in terms of dimensionless radius of curvature S_r and the clustering ratio C_r through

$$\begin{aligned} X_r =& \frac{A_{rec}}{A_c} \\ =& {S_r}^2 \left(\int_0^{\frac{C_r}{S_r\sqrt{M}}} 2\pi\bar{R}d\bar{R} + \int_{\frac{C_r}{S_r\sqrt{M}}}^{\frac{2C_r}{S_r\sqrt{3M}}} \left(2\pi - 4\arccos\frac{C_r}{S_r\sqrt{M}\bar{R}}\right)\bar{R}d\bar{R} \right. \\ &+ \int_{\frac{2C_r}{S_r\sqrt{3M}}}^{\frac{1}{S_r\sqrt{M}}} \left(\frac{5\pi}{3} - 2\arccos\frac{C_r}{S_r\sqrt{M}\bar{R}}\right)\bar{R}d\bar{R} \\ &+ \int_{\frac{1}{S_r\sqrt{M}}}^{\frac{2}{S_r\sqrt{4M-M{C_r}^2}}} \left(\frac{5\pi}{3} - 2\arccos\frac{C_r}{S_r\sqrt{M}\bar{R}} - 8\arccos\frac{1}{S_r\sqrt{M}\bar{R}}\right)\bar{R}d\bar{R} \\ &\left. + \int_{\frac{2}{S_r\sqrt{4M-M{C_r}^2}}}^{\bar{R}_n} \left(\frac{2\pi}{3} - 4\arccos\frac{1}{S_r\sqrt{M}\bar{R}}\right)\bar{R}d\bar{R} \right), \end{aligned} \tag{4}$$

where $M = \frac{2}{\sqrt{3}} + \frac{{C_r}^2}{\sqrt{3}} + C_r\sqrt{4 - {C_r}^2}$. Here too the integration steps are similar to Eq. (3). In this case, the final value of $\bar{R}_n$ is $\frac{2}{S_r\sqrt{3M}}$.

3 Results and discussion

The parameters used in this work are related to the physical processes associated with the recrystallization. This section describes the results obtained from simulations by varying these parameters. We also illustrate the ability of the proposed model in describing the influence of physical processes on the recrystallization kinetics. The instantaneous radius of a single nucleus $\bar{R}$ is calculated as a function of $\bar{t}$ by solving the Eq. (1) using an explicit forward finite difference method. Subsequently, the recrystallized area fraction as a function of $\bar{t}$ is calculated using the equations for A_{rec}. The recrystallization kinetics in the present modeling approach is dependent on the parameters: τ, ξ, M, E_i, R_c and S_r. From Eqs. (3) and (4) it is seen that the temporal evolution of X_r as function of $\bar{t}$ is determined directly by the parameters: $\bar{\tau}$, ξ and S_r. The other parameters: M, E_i, R_c determine the functional dependency between $\bar{t}$ and actual time t.

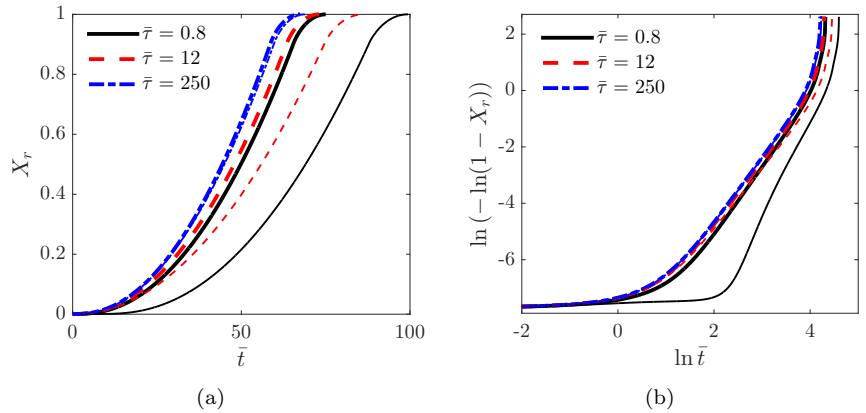

(a) (b)

Fig. 3 (a) Recrystallized fraction X_r vs. $\bar{t}$ in a linear scale and (b) $\log(-\log(1-X_r))$ with $\log(\bar{t})$ for combinations of $\bar{\tau}$ and ξ. The thick lines represent $\xi = 0.10$ and the thin lines represent $\xi = 0.25$.

3.1 Effect of recovery

In this model, the recovery of the material is characterized by the recovery time constant τ and the recoverable fraction ξ of initial stored energy E_i. The competition between recovery and recrystallization can be analyzed by investigating the role of these two parameters on the recrystallization kinetics.

Figure 3 shows the recrystallization kinetics for different values of $\bar{\tau}$ and ξ. The recrystallization kinetics is slower for lower values of $\bar{\tau}$ for given ξ (Fig. 3(a)). The recrystallization kinetics also becomes slower for larger values of ξ. Note that the parameter τ determines the rate of decrease of stored energy due to recovery. Lower τ implies that the stored energy decreases from initial value at an earlier time. On the other hand, a higher ξ value indicates that a greater part of the initial stored energy E_i is lost due to recovery. Thus lower values of $\bar{\tau}$ and higher values of ξ indicate that the stored energy available for driving force the recrystallization process is reduced thus leading to a delay in recrystallization.

To compare our results with the JMAK analysis, we calculate an apparent Avrami exponent from our recrystallization kinetics. From the plot of $\ln(-\ln(1-X_r))$ vs $\ln \bar{t}$ shown in Fig. 3(b), it is seen that the recrystallization curve from our model is not sigmoidal. Nevertheless, the plot of $\ln(-\ln(1-X_r))$ vs $\ln \bar{t}$ is approximately linear for a significant fraction of the recrystallization process (for $X_r \in (0.01, 0.7)$). The slope of the curve in this region is taken to be an apparent Avrami exponent for our analysis. Changes in recovery parameters result in significant variations in Avrami exponent.

Figure 4 shows the variation of the Avrami exponent with $\bar{\tau}$ for different values of ξ. The Avrami exponent has a high value at low $\bar{\tau}$ value; then decreases with increasing $\bar{\tau}$ and reaches a minimum value. It increases again

before attaining a final saturation value of 2.13. The nonmonotonicity in the variation of the Avrami exponent with $\bar{\tau}$ can be explained considering the rate of recovery with respect to the recrystallization process.

In Fig. 5, the effect of recovery in relation to the recrystallization is shown with $\bar{\tau}$ for $\xi = 0.25$. The decrease in stored energy due to recovery is greater in the case of low $\bar{\tau} = 0.8$. Figure 5 shows that for $\bar{\tau} = 0.8$, recovery is completed by the time a small part of recrystallization process occurs ($X_r < 0.01$). During the remaining part of the recrystallization process, the stored energy in non-recrystallized material part remains constant at a value of 0.75 $(1 - \xi)$. Thus the decrease in stored energy due to recovery influences only the initial part of the recrystallization process ($X_r < 0.01$). Subsequently, the slope of $\ln(-\ln(1-X_r))$ vs $\ln \bar{t}$ curve is steeper (Fig. 3b) in the recrystallization regime over $0.1 < X_r < 0.7$. This results in a high calculated Avrami exponent for lower values $\bar{\tau} = 0.8$.

At higher recovery time constant values $\bar{\tau} = 12$, the decrease in stored energy due to recovery occurs over a larger period of time. For $\bar{\tau} = 12$, the decrease in stored energy due to recovery occurs up to a recrystallization fraction of $X_r < 0.4$ (Fig. 5). When the recovery period spans a greater part of the recrystallization, it results in a more gradual slope of $\ln(-\ln(1 - X_r))$ vs $\ln \bar{t}$ curve in the characteristic regime of $0.1 < X_r < 0.7$. This results in a lower value of the calculated Avrami exponent for $\bar{\tau} < 12$. For higher $\bar{\tau}$, the Avrami exponent of about 2 is calculated. Thus the minimum value of the calculated Avrami exponent depends strongly on ξ.

Finally, it is evident from Fig. 5 that if the recovery of the stored energy continues beyond the recrystallization process for a $\bar{\tau} > 100$. Thus when the recovery process is slower (higher $\bar{\tau}$), the increasing availability of stored energy to drive the growth of the nuclei results in an increase in the calculated value of the Avrami exponent.

This discussion is focused on the effects of the two parameters: the recovery time constant $\bar{\tau}$ and fraction of stored energy recovered ξ on the recrystallization. To put these in context, these recovery characteristics mostly depend on the stacking fault energy of the material [1, 2]. In metals with low stacking fault energy, the recovery associated mechanism is less dominant during the recrystallization process. However, in metals with high stacking fault energy such as aluminium and iron, significant recovery is reported. In such cases, recovery can be characterized by a combination of low $\bar{\tau}$ and high ξ.

In order to correlate our calculations with the experimental values of the stored energy which are measured throughout the domain, we plot the average stored energy (along with stored energy decay in only the deformed region for reference) in Fig. 6. The qualitative trends match the different types of recovery features reported in the literature to good accord. In low stacking fault energy materials, the reported trend in average stored energy change during recrystallization qualitatively matches the result for $\bar{\tau} = 250$ and $\xi = 0.10$ [25, 26]. For such materials, the recovery rate is small during the recrystallization process and recrystallization completes without any significant loss of stored

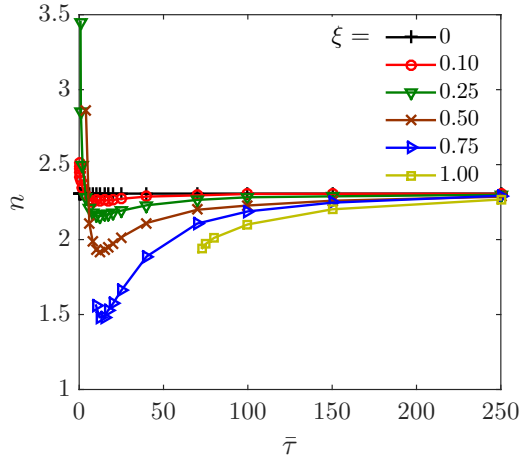

Fig. 4 Variation of Avrami exponent n with the recovery time constant $\bar{\tau}$ for different values of recovered stored energy fraction ξ. As noted in the text, the Avrami exponent is calculated for recrystallization fraction in the range $0.1 < X_r < 0.7$.

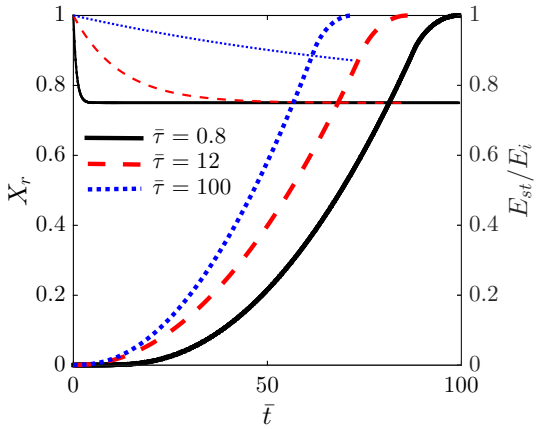

Fig. 5 Recrystallization rate $X_r(t)$ for different recovery kinetics $E_{st}(t)$ for $\xi = 0.25$. The recrystallization curves are shown with thick lines whereas the recovery curves are shown with thin lines.

energy due to recovery. Consequently, there is hardly any effect of recovery on the recrystallization kinetics.

On the other hand, materials with high stacking fault energy show qualitatively different characteristics. Such materials (e.g. Al [25, 27] and low carbon steel [28]) qualitatively follow the results with $\bar{\tau} = 4, \xi = 0.25$ and $\bar{\tau} = 40, \xi = 0.50$. These two cases depict the situations in which a considerable amount of stored energy is recovered. As a result, recovery could strongly affect the recrystallization kinetics.

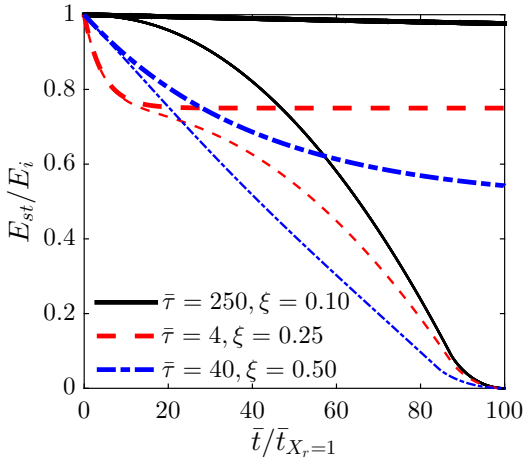

Fig. 6 Decay of stored energy for different recovery parameters $\bar{\tau}$ and ξ. Thick lines indicate the stored energy in the deformed regions whereas the thin lines indicate the average stored energy over the whole domain.

Table 1 Critical values of the recovery parameters for cessation of recrystallization.

Recovery parameter	Critical values						
ξ	0	0.25	0.50	0.75	0.90	0.95	1.00
$\bar{\tau}$	0	0.8	4	8	15	26	73

Finally, we note that the Avrami exponent values in Fig. 4 are calculated only for $\bar{\tau}$ greater than some critical values for different ξ. Below these critical values, recovery decreases the driving force such that the nuclei stop growing. This suggests that complete recrystallization cannot be achieved if the material possesses a high tendency for recovery (a combination of low $\bar{\tau}$ and high ξ). This is borne out by experimental studies [2]. The critical $\bar{\tau}$ values are given in Table 1.

3.2 Effect of temperature and deformation amount

It is well known that the recrystallization rate increases with both temperature and amount of deformation [1]. Increase in temperature increases velocity of the grain boundary during recrystallization. The stored energy E_i provides additional driving force for the GB motion and the mobility parameter M determines the GB velocity [2, 11]. In this model, the parameters M and E_i are treated via the product $\phi = ME_i$, and this product acts as a governing parameter of recrystallization kinetics. Figure 7 shows the recrystallization kinetics for different values of ϕ. The recrystallization process is seen to accelerate with increase of ϕ, i.e. due to an increase in either mobility or the stored energy

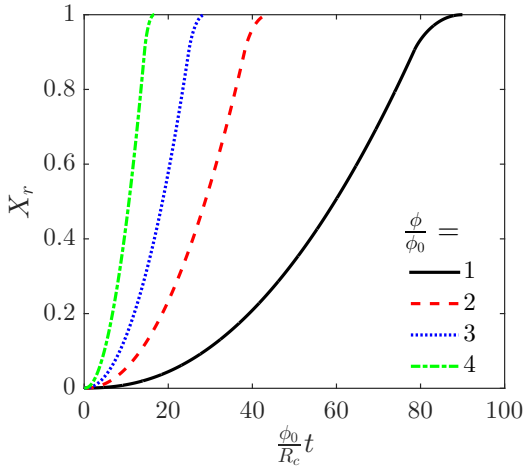

Fig. 7 Recrystallization kinetics for different values of $\phi(= ME_i)$. The recrystallization rate increases with the product of mobility and initial stored energy.

such that the product increases which is qualitatively similar to experimental observations [1].

Figure 8 shows envelopes of the values of τ and ξ below which complete recrystallization does not occur due to recovery. The envelopes are at higher values with decreasing values of ϕ. This implies that complete recrystallization can be ensured with either decrease of energy release or rate of recovery i.e., a decrease of the recoverable fraction ξ of stored energy or an increase of τ. It can conversely be inferred that complete recrystallization is inhibited at lower temperatures and lower deformation amounts if the same recovery characteristic is maintained.

3.3 Effect of clustering

In this model, we adopt a simple approach to describe the effect of clustered nucleation using a single parameter C_r which is defined as the ratio of separation of particles in a cluster to the separation distance of the clusters $= r_3/R_3$. From Fig. 2(b) we can see that the clustering parameter C_r decreases from value 1 with increased clustering. The recrystallization kinetics is plotted in Fig. 9 for different C_r values for two different value of the nuclei density $S_r = R_c/\sqrt{A_c}$. It is observed the recrystallization rate decreases with increased clustering. At higher nuclei densities, the recrystallization rate increases. Such a variation in nuclei density generally occurs with changes in the amount of deformation of the material [3]. The variation of Avrami exponent with C_r is plotted in Fig. 10 for two different values of densities of the nuclei, S_r. It can be observed that Avrami exponent increases with increasing C_r, and a maximum is attained

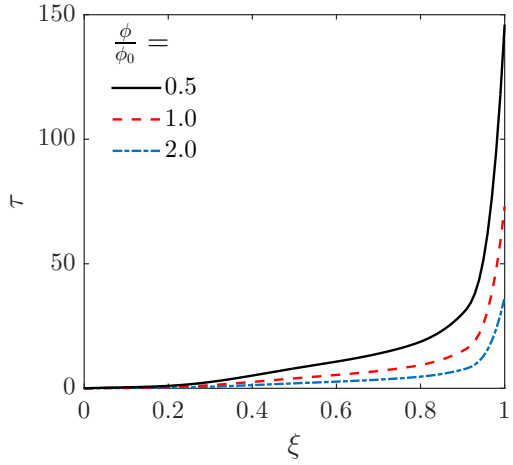

Fig. 8 Each of the curves represents the upper bound of values of ξ and τ for which complete recrystallization does not occur. The envelope is at higher values for lower values of ϕ.

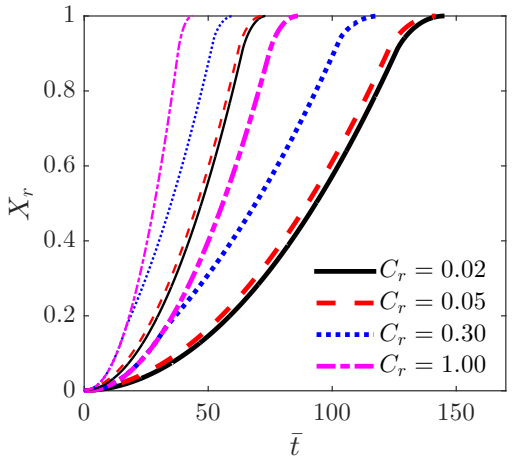

Fig. 9 Recrystallization kinetics for different clustering parameter (C_r) with two different conditions of $S_r = 0.01$ (represented by thick lines) and $S_r = 0.02$ (represented by thin lines).

near C_r value 1. The observed non-monotonicity in the Avrami exponent is due to the first impingement effect of the nucleus clusters.

3.4 Comparison with a phase field model

In this section, we briefly compare the results of the mean field model with multiorder parameter phase field (PF) simulations. A multiorder parameter

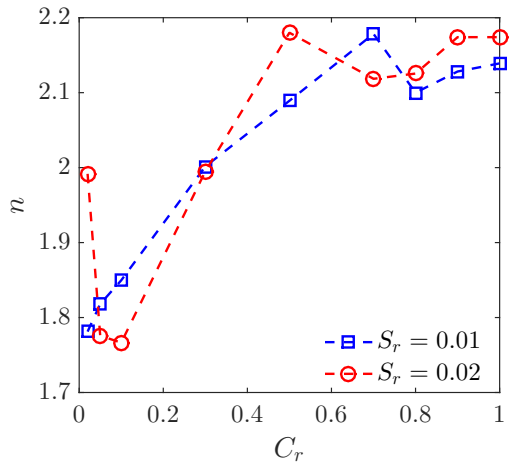

Fig. 10 Variation of Avrami exponent n with clustering ratio (C_r) for two different values of S_r.

PF model developed in our previous work [29, 23] was used for these simulations. The effect of the stored energy is accounted for by changing the depth of the double well potential (for details, see [29, 23]). The stored energy decay effect due to recovery is incorporated by appropriately changing the PF parameters. The simulations are carried out in a 600×600 domain. The simulations are performed for uniform and random distributions of initially circular nuclei. Time scaling is performed to normalize the results of the phase field simulations.

Figure 11 shows the comparison of the results obtained from the mean field and PF models for uniform distribution of nuclei and different recovery characteristics. The agreement between phase field model and mean field model is quite good for a range of recovery characteristics.

Next, we consider a random distribution of nuclei in the PF simulations. In Fig. 12 the initial distribution of nuclei is characterized through the distribution of the distances between adjacent nuclei obtained from a Voronoi tessellation. Figure 13 shows the recrystallization kinetics obtained from the PF simulation with the mean field results for different C_r values. The recrystallization kinetics from the PF simulations is a superposition of several impingement events of different C_r values occurring at different times. Therefore the net effect is that the recrystallization curve from the PF simulations matches the mean field model kinetics for $C_r \in (0.3, 0.5)$ over most of the recrystallization process. Thus the partial contributions of RVEs with different C_r seem to affect the recrystallization kinetics in case of the random distribution of nuclei.

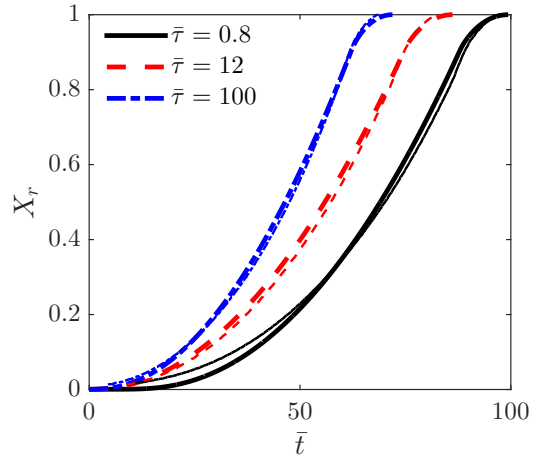

Fig. 11 Comparison of the recrystallization kinetics from mean field model (represented by thick lines) with phase field model (represented by thin lines) for uniform distribution of nuclei with recovery parameter $\xi = 0.25$.

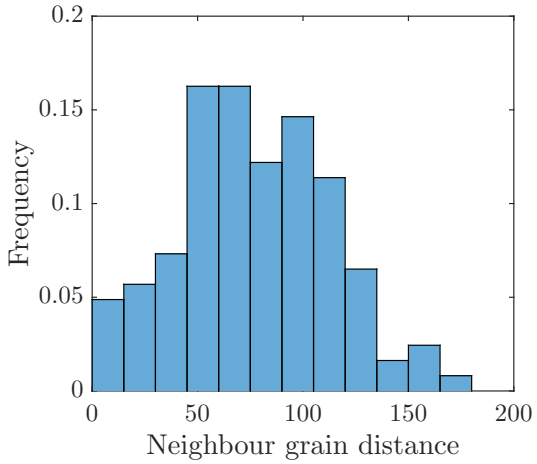

Fig. 12 Initial distribution of distance between adjacent nuclei used in the phase field simulation of the random distribution of nuclei.

4 Conclusions

We have presented a physically based model of recrystallization kinetics in this work. The mobility of the grain boundary, initial stored energy, nuclei density, and the characteristics of recovery are considered in the model. For a description of recovery, an exponential form of energy decay has been adopted. Any enhancement in energy decay due to recovery is predicted to increase the recrystallization completion time. In this case, the Avrami exponent is not

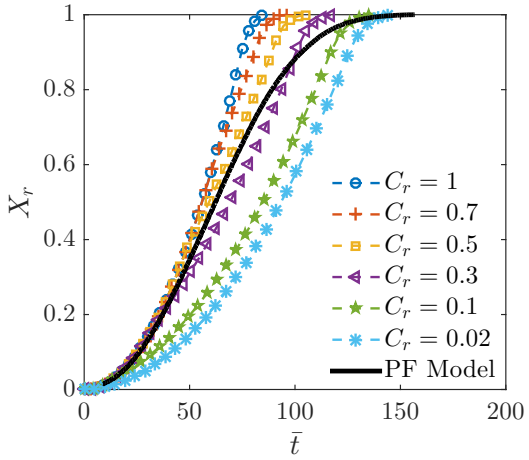

Fig. 13 Comparison of recrystallization curve from phase field model with random distribution with the recrystallization curves from mean field model with different clustering ratio C_r values.

found to be a monotonic function of the recovery rate. The various regimes of competition between recovery and recrystallization, as reported in the literature, are also well captured by the present model. The model predicts that if the recovery is greater than a critical level, the recrystallization process ceases. A simple RVE based model of clustering of the nuclei reveals that the recrystallization process slows down as clustering increases. The present work only considers an idealized distribution with a consideration of the impingement between the growing strain free grains. We find that it provides excellent insights into the recrystallization kinetics and compares well with phase field simulations of recrystallization. Future extensions of this model could consider the effect of other kinds of RVEs and other random distributions of the nuclei.

Acknowledgements:

One of the authors (Partha Sarathi De) acknowledges the award of Institute Post Doctoral Fellowship from Indian Institute of Technology Madras for carrying out the current research work.

Compliance with Ethical Standards:

Funding: No funding was received for the current study.

Conflict of Interest: The authors declare that they have no conflict of interest.

References

1. Humphreys F, Hatherly M (2004) Chapter 7 - recrystallization of single-phase alloys. In: Humphreys F, Hatherly M (eds) Recrystallization and Related Annealing Phenomena (Second Edition), second edition edn, Elsevier, Oxford, pp 215 – IV, DOI https://doi.org/10.1016/B978-008044164-1/50011-6, URL https://www.sciencedirect.com/science/article/pii/B9780080441641500116
2. Raabe D (2014) 23 - recovery and recrystallization: Phenomena, physics, models, simulation. In: Laughlin DE, Hono K (eds) Physical Metallurgy (Fifth Edition), fifth edition edn, Elsevier, Oxford, pp 2291 – 2397, DOI https://doi.org/10.1016/B978-0-444-53770-6.00023-X, URL https://www.sciencedirect.com/science/article/pii/B978044453770600023X
3. Rios PR, Siciliano Jr F, Sandim HRZ, Plaut RL, Padilha AF (2005) Nucleation and growth during recrystallization. Materials Research 8:225 – 238, DOI https://doi.org/10.1590/S1516-14392005000300002, URL http://www.scielo.br/scielo.php?script=sci_arttext&pid=S1516-14392005000300002&nrm=iso
4. Doherty R, Hughes D, Humphreys F, Jonas J, Jensen D, Kassner M, King W, McNelley T, McQueen H, Rollett A (1997) Current issues in recrystallization: a review. Materials Science and Engineering: A 238(2):219 – 274, URL http://www.sciencedirect.com/science/article/pii/S0921509397004243
5. Lü Y, Molodov DA, Gottstein G (2011) Recrystallization kinetics and microstructure evolution during annealing of a cold-rolled fe–mn–c alloy. Acta Materialia 59(8):3229 – 3243, DOI https://doi.org/10.1016/j.actamat.2011.01.063, URL http://www.sciencedirect.com/science/article/pii/S1359645411000796
6. Medina SF, Quispe A (2001) Improved model for static recrystallization kinetics of hot deformed austenite in low alloy and nb/v microalloyed steels. ISIJ International 41(7):774–781, DOI 10.2355/isijinternational.41.774
7. Laasraoui A, Jonas JJ (1991) Recrystallization of austenite after deformation at high temperatures and strain rates—analysis and modeling. Metallurgical Transactions A 22(1):151–160, DOI 10.1007/BF03350957, URL https://doi.org/10.1007/BF03350957
8. Vandermeer RA, Rath BB (1989) Microstructural modeling of recrystallization in deformed iron single crystals. Metallurgical Transactions A 20(10):1933–1942, DOI 10.1007/BF02650280, URL https://doi.org/10.1007/BF02650280
9. Vandermeer R, Jensen DJ (2001) Microstructural path and temperature dependence of recrystallization in commercial aluminum. Acta Materialia 49(11):2083 – 2094, DOI https://doi.org/10.1016/S1359-6454(01)00074-X, URL http://www.sciencedirect.com/science/article/pii/S135964540100074X

10. Oyarzábal M, de Guerenu AM, Gutiérrez I (2008) Effect of stored energy and recovery on the overall recrystallization kinetics of a cold rolled low carbon steel. Materials Science and Engineering: A 485(1):200 – 209, DOI https://doi.org/10.1016/j.msea.2007.07.077, URL http://www.sciencedirect.com/science/article/pii/S0921509307015080
11. Stüwe H, Padilha A, Siciliano F (2002) Competition between recovery and recrystallization. Materials Science and Engineering: A 333(1):361 – 367, URL http://www.sciencedirect.com/science/article/pii/S0921509301018603
12. Storm S, Jensen DJ (2009) Effects of clustered nucleation on recrystallization. Scripta Materialia 60(7):477 – 480, DOI https://doi.org/10.1016/j.scriptamat.2008.11.020, URL http://www.sciencedirect.com/science/article/pii/S1359646208007914
13. Villa E, Rios PR (2009) Transformation kinetics for nucleus clusters. Acta Materialia 57(13):3714 – 3724, DOI https://doi.org/10.1016/j.actamat.2009.04.014, URL http://www.sciencedirect.com/science/article/pii/S1359645409002328
14. Vandermeer R, Juul Jensen D (1998) The migration of high angle grain boundaries during recrystallization. Interface Science 6(1):95–104, DOI 10.1023/A:1008668604733, URL https://doi.org/10.1023/A:1008668604733
15. Wu G, Jensen DJ (2005) Recrystallisation kinetics of aluminium aa1200 cold rolled to true strain of 2. Materials Science and Technology 21(12):1407–1411, DOI 10.1179/174328405X71602, URL https://doi.org/10.1179/174328405X71602, https://doi.org/10.1179/174328405X71602
16. Speich G, Fisher R (1966) Recrystallization, grain growth and textures. Am Soc Metals, Metals Park, Ohio p 563
17. Clemente R, Saleh A (2002) Crystallization kinetics: A solution for geometrical impingement. Physical Review B - Condensed Matter and Materials Physics 65(13):1321021–1321023, DOI 10.1103/PhysRevB.65.132102, URL https://www.scopus.com/inward/record.uri?eid=2-s2.0-0036537870&doi=10.1103%2fPhysRevB.65.132102&partnerID=40&md5=d44808e649b6925fb468b9af2d28169c, cited By 6
18. Van Siclen C (1996) Random nucleation and growth kinetics. Physical Review B - Condensed Matter and Materials Physics 54(17):11845–11848, DOI 10.1103/PhysRevB.54.11845, URL https://www.scopus.com/inward/record.uri?eid=2-s2.0-0012985106&doi=10.1103%2fPhysRevB.54.11845&partnerID=40&md5=488b3b53f8542cd5572d614f708082dc, cited By 53
19. Almansour A, Matsugi K, Hatayama T, Yanagisawa O (1996) Modeling of growth and impingement of spherical grains. Materials Transactions, JIM 37(10):1595–1601, DOI 10.2320/matertrans1989.37.1595, URL https://www.scopus.com/inward/record.uri?eid=2-s2.0-0030264399&doi=10.2320%2fmatertrans1989.37.1595&partnerID=40&md5=09ebb2581f163154f7705f304f79c3be, cited By 17

20. Gokhale A, Iswaran C, Dehoff R (1980) Application of microstructure modelling to the kinetics of recrystallization. Metallurgical Transactions A 11(8):1377–1383, DOI 10.1007/BF02653492, URL https://www.scopus.com/inward/record.uri?eid=2-s2.0-0019045280&doi=10.1007%2fBF02653492&partnerID=40&md5=31b17e11031792109f3be52a7bf5fab0, cited By 29
21. Mukunthan K, Hawbolt E (1996) Modeling recovery and recrystallization kinetics in cold-rolled ti-nb stabilized interstitial-free steel. Metallurgical and Materials Transactions A: Physical Metallurgy and Materials Science 27(11):3410–3423, DOI 10.1007/BF02595434, URL https://www.scopus.com/inward/record.uri?eid=2-s2.0-0030285515&doi=10.1007%2fBF02595434&partnerID=40&md5=0cdb120306451b6d9cc88158e415ae95, cited By 57
22. Rios P (1997) Modeling time dependence of the average interface migration rate in site-saturated recrystallization. Metallurgical and Materials Transactions A: Physical Metallurgy and Materials Science 28(4):939–946, DOI 10.1007/s11661-997-0224-1, URL https://www.scopus.com/inward/record.uri?eid=2-s2.0-0031118020&doi=10.1007%2fs11661-997-0224-1&partnerID=40&md5=d4dcae9f3fe3f54c0632412c0db651f1, cited By 14
23. Athreya CN, Mukilventhan A, Suwas S, Vedantam S, Sarma VS (2017) Influence of the mode of deformation on recrystallisation kinetics in nickel through experiments, theory and phase field model. Philosophical Magazine 97(34):3211–3228, DOI 10.1080/14786435.2017.1370146, URL https://doi.org/10.1080/14786435.2017.1370146, https://doi.org/10.1080/14786435.2017.1370146
24. Fan D, Chen LQ (1997) Computer simulation of grain growth using a continuum field model. Acta Materialia 45(2):611 – 622, DOI https://doi.org/10.1016/S1359-6454(96)00200-5, URL http://www.sciencedirect.com/science/article/pii/S1359645496002005
25. Furu T, Marthinsen K, Nes E (1990) Modelling recrystallisation. Materials Science and Technology 6(11):1093–1102, DOI 10.1179/mst.1990.6.11.1093, URL https://doi.org/10.1179/mst.1990.6.11.1093, https://doi.org/10.1179/mst.1990.6.11.1093
26. Rohatgi A, Vecchio K (2002) The variation of dislocation density as a function of the stacking fault energy in shock-deformed fcc materials. Materials Science and Engineering: A 328(1):256 – 266, DOI https://doi.org/10.1016/S0921-5093(01)01702-6, URL http://www.sciencedirect.com/science/article/pii/S0921509301017026
27. Pimenta Jr FC, Arruda ACF, Padilha AF (1986) Resistance to recrystallization in al-1% mn alloys. Zeitschrift für Metallkunde 77(8):522–528
28. Ray RK, Hutchinson B, Ghosh C (2011) 'back-annealing' of cold rolled steels through recovery and/or partial recrystallisation. International Materials Reviews 56(2):73–97, DOI 10.1179/095066010X12646898728444, URL https://doi.org/10.1179/095066010X12646898728444, https://doi.org/10.1179/095066010X12646898728444

29. Athreya CN, Mukilventhan A, Suwas S, Vedantam S, Sarma VS (2018) Influence of the mode of deformation on recrystallisation behaviour of titanium through experiments, mean field theory and phase field model. Modelling and Simulation in Materials Science and Engineering 26(3):035004, DOI 10.1088/1361-651x/aaa6a4, URL https://doi.org/10.1088%2F1361-651x%2Faaa6a4

A Calculation of recrystallized fraction in uniform distribution of nuclei

In order to calculate the growth after impingement, the circumference of each grain is taken as sections of mobile boundaries. The outward movement of these sections consume the rest of the deformed matrix. It is assumed that each of the boundary sections move following the same kinetics as in Eq. (1). The driving forces on each of the boundary sections are taken to arise from curvature and stored energy differences. The recrystallized area is the area of white region in each representative hexagonal volume element in Fig. 1. After impingement the recrystallized area A_{rec} can be calculated as

$$A_{rec} = 2\pi \int_0^{R_1} RdR + \int_{R_1}^{R_n} \left(2\pi - 12 \arccos \frac{R_1}{R}\right) RdR, \tag{5}$$

where R_n is current radius of curvature and $2R_1$ is the distance between center of two nuclei. Prior to impingement, when R_n is lower than R_1, then the first term of integration gives the value of A_{rec}; the second term is included after impingement when $R_n > R_1$. The maximum value of R_n can be derived from Fig. 1 to be $\frac{2}{\sqrt{3}R_1}$ and this marks the completion of the recrystallization of the RVE. The recrystallized area fraction X_r can be simply calculated by dividing the recrystallized area A_{rec} by final area of a grain i.e. area A_c of representative hexagonal volume element as shown in Figs. 1b and c. By replacing R with $\bar{R}$, X_r can be expressed as

$$\begin{aligned} X_r = \frac{A_{rec}}{A_c} = {S_r}^2 \Bigg(& 2\pi \int_0^{\frac{1}{\sqrt[4]{12}S_r}} \bar{R}d\bar{R} \\ & + \int_{\frac{1}{\sqrt[4]{12}S_r}}^{\bar{R}_n} \left(2\pi - 12 \arccos\left(\frac{1}{\sqrt[4]{12}S_r\bar{R}}\right)\right) \bar{R}d\bar{R} \Bigg), \end{aligned} \tag{6}$$

where $S_r = \frac{R_c}{\sqrt{A_c}}$. The limiting value of $\bar{R}_n$ at the completion of recrystallization is $\frac{\sqrt{2}}{\sqrt[4]{27}S_r}$ corresponding to R_n value of $\frac{2}{\sqrt{3}R_1}$ and S_r is related to both critical nuclei radius and nuclei density $\frac{1}{\sqrt{A_c}}$.